Hexagons become second if symmetry is broken

Bert Reimann[1], Reinhard Richter[1], Holger Knieling[1], Rene Friedrichs[2] and Ingo Rehberg[1]
[1] *Physikalisches Institut, Experimentalphysik V, Universität Bayreuth, D-95440 Bayreuth, Germany, and*
[2] *FNW/ITP, Otto-von-Guericke-Universität, D-39016 Magdeburg, Germany*
(Dated: 1st October 2004)

Pattern formation on the free surface of a magnetic fluid subjected to a magnetic field is investigated experimentally. By tilting the magnetic field the symmetry can be broken in a controllable manner. When increasing the amplitude of the tilted field, the flat surface gives way to liquid ridges. A further increase results in a hysteretic transition to a pattern of stretched hexagons. The instabilities are detected by means of a linear array of magnetic hall sensors and compared with theoretical predictions.

PACS numbers: 05.45-a, 47.54+r, 47.52

Pattern formation in isotropic systems is more complicated than in anisotropic ones: One of the hallmarks of isotropic systems is the possibility to bifurcate to hexagons from an unstructured ground state, which is due to the existence and interaction of 3 degenerate wave numbers [1]. This situation is *structurally unstable*, however: The smallest distortion of this symmetry acts as a singular perturbation and will lead to a qualitatively different instability, namely a primary bifurcation to a stripe like pattern. A specific example has recently been calculated in detail [2] for a magnetic fluid [3]. In the ideal isotropic system, hexagons will occur under the influence of a magnetic field which is perfectly normal with respect to the fluid surface [4]. The slightest change of the orientation of the magnetic field is predicted to change this subcritical transition: Ridges appear supercritically via the primary bifurcation. Their interaction with waves along the less-favoured direction gives rise to "stretched" hexagons via a secondary bifurcation.

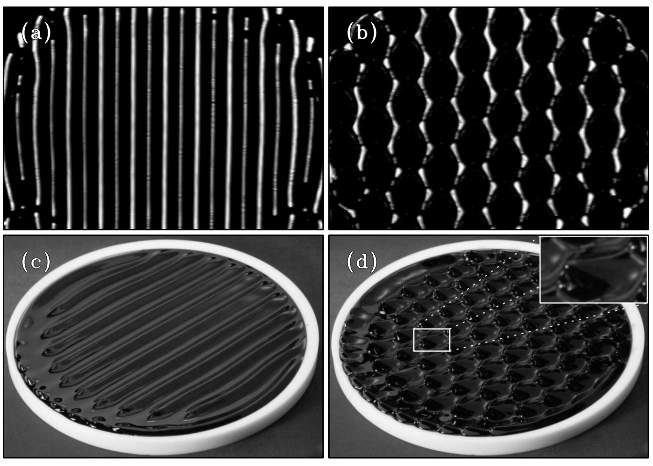

FIG. 1: Surface patterns of magnetic fluid in a magnetic field tilted by the angle $\varphi = 23^0$ to the vertical. Surface reflections of the liquid ridges for the verical induction $\bar{B}$ =20 mT (a) and of the tilted crests for $\bar{B}$ =32 mT (b). The side view of the patterns is presented in (c) and (d), respectively.

A first observation of liquid ridges was reported in Ref. [5]. In this paper we present a quantitative characterization of the primary bifurcation to liquid ridges and a secondary bifurcation to a pattern of stretched hexagons, as shown in Fig.1, via use of a magnetic measurement technique. Specifically, we measure the threshold induction B_p and B_s for the primary and secondary instability for various angles of tilt φ. The measurements of $B_\mathrm{p}(\varphi)$ agree with the theoretical prediction if the nonlinear magnetization curve of the magnetic fluid used in the experiment is taken into account.

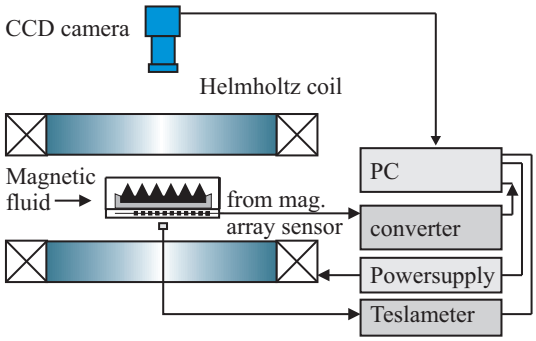

FIG. 2: Scheme of the experimental setup.

Our experimental setup is shown in Fig. 2. A cylindrical vessel with an edge machined from Teflon® with a diameter of 12 cm and a depth of 2 mm is brimful filled with fluid and is situated in the center of a pair of Helmholtz coils. For details see Ref. [6]. The axis of the coils can be tilted against the vertical by an angle $\varphi = [0^0, 90^0]$. The experiments are performed with the magnetic fluid EMG 909 Lot F061998B (Ferrotec Corp.), with $\mu_r = 2.11$. A charge-coupled-device (CCD) camera is recording the patterns from above. In order to measure the *amplitude* of the steep crests a linear array of 32 hall sensors was mounted 1.78 ± 0.1 mm below the bottom of the dish. By this technique the local increase of the magnetic induction below a liquid crest is utilized to measure its amplitude. The sensors communicate via 32 amplifiers

and a bus with the PC. Details of this method are presented elsewere [7]. For calibration purpose a commercial Hall probe (Group3-LPT-231) in combination with the digital teslameter (DTM 141) was used.

The magnetic field is tilted towards the x-axis. Increasing the magnetic induction, we observe a transition from the flat layer of magnetic fluid to the pattern of liquid ridges, displayed in Fig.1a,c. The wave vector of the pattern is oriented along the y-axis and thus perpendicular to the horizontal field component. The vertical component of the local magnetic induction was measured by means of the sensor array oriented parallel to the wave vector. In order to reduce the spatial inhomogeneities of the magnetization caused by the finite container size, the spatial variation measured at a subcritical induction of 20.5 mT is substracted. The ensuing local induction $B(x)$ is presented in Fig. 3 for different values of the applied magnetic field, measured at the tilt angle $\varphi = 32^0$. The open circles mark the data, the solid line gives the least square fit to

$$B(x) = A \cdot \cos(kx - \psi) + \bar{B}. \qquad (1)$$

Here A denotes the modulation amplitude, k the absolute value of the wave vector, ψ the phase, and $\bar{B}$ the mean value of the induction.

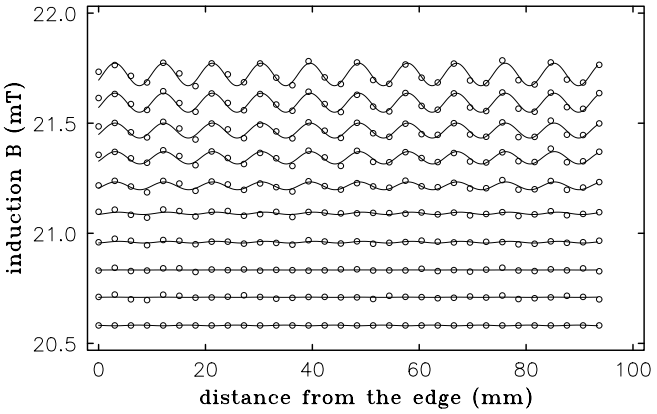

FIG. 3: Profiles of $B(x)$, for different values of the applied magnetic field. The open circles mark the data, the solid lines the fits by Eq. (1).

The square of the modulation amplitude A is plotted in Fig. 4 versus the control parameter $\bar{B}$. The monotonous increase after a threshold B_p is characteristic for a supercritical bifurcation. It can be described by the solution of the stationary amplitude equation [1]

$$0 = \epsilon_\mathrm{p} A - gA^3 + b. \qquad (2)$$

In accordance with the symmetry of the problem $\epsilon_\mathrm{p} = (\bar{B}^2 - B_\mathrm{p}^2)/B_\mathrm{p}^2$ was selected to be the dimensionless bifurcation parameter. g is the cubic coefficient a scaling-, and b a imperfection parameter. The solid line in Fig.4

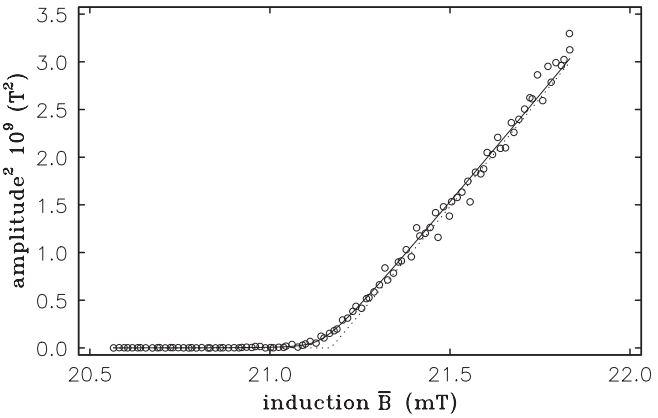

FIG. 4: Square of the modulation amplitude of the liquid ridges versus the mean magnetic induction $\bar{B}$ of the array detector. For details see text.

gives the fit of the experimental data by the solution of Eq.(2). We obtain $B_\mathrm{p} = 21.17\mathrm{mT}$, $g = 21.16\mathrm{mT}^{-2}$, and the slight imperfection $b = 4.3 \cdot 10^{-5}\mathrm{mT}$. The dotted line displays the solution without imperfection ($b = 0\mathrm{mT}$).

Increasing the controll parameter further initiates a secondary instability to the stretched hexagonal pattern as displayed in Fig.1b,d. The blow–up in (d) indicates that the crests riding on top of the ridges are asymmetric with respect to the wave vector of the ridges. Thus the pattern (of stretched hexagons) lacks any non–trivial rotational symmetry.

For a quantitative analysis of the secondary instability a series of 400 measurements of the local induction $B(x)$ has been performed for $\varphi = 23^0$. For clarity Fig. 5a (b) is presenting only every 20th line for a quasistatic increase (decrease) of the control parameter $\bar{B}$, respectively. In order to detect both, the ridges and the crests, the sensor line is now oriented with an angle $\omega = (75.8 \pm 0.05)^0$ to the y-axis. In this way it is covering $2\,\frac{1}{2}$ ridges, which can be recognized in the lower part of the plots. For $B \approx 22\,\mathrm{mT}$ the transition to the stretched hexagons occurs.

A mathematical characterization of the stretched hexagons can be obtained as follows. In a stretched-hexagonal pattern the wave vectors fulfill the side condition $-\vec{k_1} = \vec{k_2} + \vec{k_3}$ and $\bar{k} = |\vec{k_2}| = |\vec{k_3}|$. With the abbreviations $k = |\vec{k_1}|$, $n = \bar{k}/k$ and $\tilde{b} = \sqrt{4n^2 - 1}$ the wave vectors read $\vec{k_1} = k(0, 1, 0)$, $\vec{k_2} = -\frac{k}{2}(-\tilde{b}, 1, 0)$, and $\vec{k_3} = -\frac{k}{2}(\tilde{b}, 1, 0)$ which coincide for $n = 1$ with the vectors for a regular hexagonal pattern. The amplitude of the ridges A_0^R and of the stretched-hexagonal pattern A_0^H can be combined to the amplitude of the over-all pattern

$$A(\vec{x}) = A_0^R \cos \vec{k}_1 \vec{x} + \frac{A_0^H}{3} \sum_{i=1}^{i=3} \cos \vec{k}_i \vec{x}\,. \qquad (3)$$

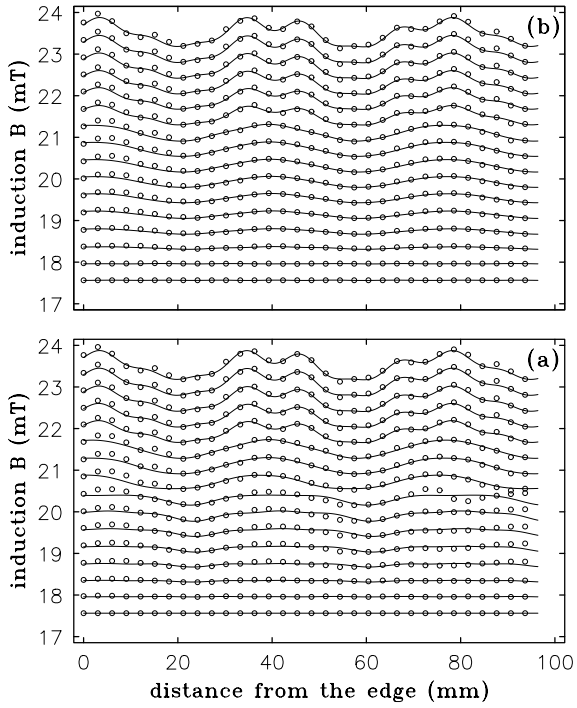

FIG. 5: Local magnetic induction for increasing (a) and decreasing (b) control parameter $\bar{B}$ and $\varphi = 23^0$. The solid lines give the fit by Eq. (8).

A cut through this pattern is given by

$$\vec{x}_M = \vec{x}_0 + t \cdot \vec{e} \tag{4}$$

where t denotes the distance from the starting point $\vec{x}_0 = (x_0, y_0, 0)$ of the sensor line and $\vec{e} = (\sin\omega, \cos\omega, 0)$ its unity vector of orientation. Plugging Eq.(4) in Eq.(3) yields

$$A(\vec{x}_M) = A(t) = A_0^R R(t) + A_0^H H(t). \tag{5}$$

for the amplitude along the sensor line. Here

$$R(t) = \cos\left(k(y_0 + t\cos\omega)\right) \tag{6}$$

gives the contribution of the ridges, and

$$\begin{aligned} H(t) \;=\; & \frac{1}{3}\left[\cos(k(y_0 + t\cos\omega)) + \cos(k(\Phi^\star + t\Psi^\star))\right. \\ & \left. + \cos(k(\Phi + t\Psi))\right] \end{aligned} \tag{7}$$

the contribution of the hexagons. Here $\Phi = \frac{1}{2}(bx_0 + y_0)$, $\Psi = \frac{1}{2}(b\sin\omega + \cos\omega)$, $\Phi^\star = \frac{1}{2}(bx_0 - y_0)$ and $\Psi^\star = \frac{1}{2}(b\sin\omega - \cos\omega)$ are abbreviations. For small amplitudes Eq.(5) is sufficient, but for higher amplitudes it is important to take into account the higher harmonics $k_m = m \cdot k$ with $m = 1, 2, ...$ The surface is than given by

$$A(t) = \sum_{m=1}^{M_R} A_0^{R_m} R_m(t) + \sum_{m=1}^{M_H} A_0^{H_m} H_m(t). \tag{8}$$

This model is fitted to the data by four nonlinear parameters, which are the wave number k of the ridges, the starting point $\vec{x_0} = (x_0, y_0)$ of the sensor line, and the stretching factor n of the hexagonal pattern. The amplitudes A_0^R and A_0^H are linear parameter of the basic functions $R(t)$ and $H(t)$. The solid lines in Fig.5 give the best fit by Eq.(8) taking into account the basic mode of the ridges ($M_R = 1$) and the first two of the hexagons ($M_H = 2$).

From this fit the amplitude A_0^H of the hexagons can be extracted. It is plotted in Fig.6 vs. the control parameter $\bar{B}$. The open squares (circles) mark the data for an increase (decrease) of $\bar{B}$, respectively. The hysteresis is characteristic for a subcritical bifurcation, which has been predicted for the transition from ridges to stretched hexagons [2].

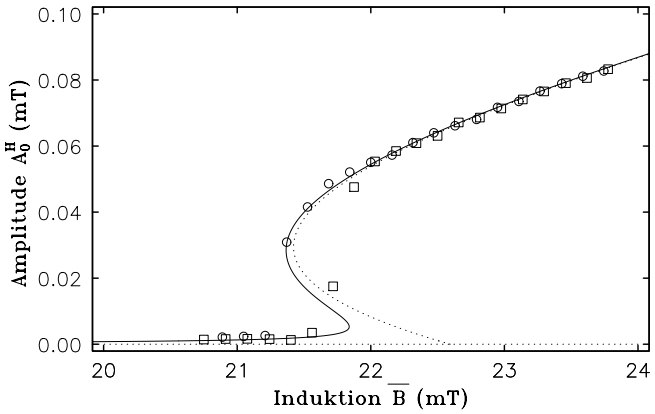

FIG. 6: Amplitude $A_0^{\rm H}$ of the stretched hexagonal pattern versus the applied magnetic induction. The open squares (circles) denote the measured amplitude under increase (decrease) of the induction, respectively. For clarity only every 10th point is shown. The solid (dotted) line give the fit by Eq.(9) with $b = 1.6 \cdot 10^{-4}$mT ($b = 0$mT), respectively. For the other parameters we obtained $B_{\rm s} = 22.594$mT, $\gamma_1 = 7.6{\rm mT}^{-1}$, $\gamma_2 = 0.9{\rm mT}^{-1}$, and $g = 116.31{\rm mT}^{-2}$.

Next we describe the amplitude $A_H \equiv A_0^H$ of the hexagons after the secondary bifurcation at $\epsilon_{\rm S} = (\bar{B}^2 - B_{\rm S}^2)/B_{\rm P}^2$. In the spirit of a weakly nonlinear analysis slightly above $\epsilon_{\rm S}$ we use the amplitude equation

$$0 = \epsilon A_H + \gamma_1(1 + \gamma_2\epsilon_S)A_H^2 - gA_H^3 + b_S. \tag{9}$$

In this experimental paper the coefficients in Eq.(9) have been obtained by a fit to the measurements in order to circumvent their tedious calculation from the basic equations. To avoid the ambiguity of $A_H(\bar{B})$ in the hysteretic regime, $\bar{B}(A_H)$ was fitted to the data according to Ref. [9]. The result of the fit is presented in Fig.6 by a solid line, while the dashed line gives the solution for the same parameters, however with $b_S = 0$.

For decreasing $\bar{B}$ the system follows the solid line very well down to the saddle-node. For increasing $\bar{B}$ the agreement is less convincing in the bistable regime. Here the impact of the edges [10] seems to penetrate the interior of the dish much stronger. As a consequence the analysis by Eq.(9) is not sufficient in this regime - see also Fig.5a.

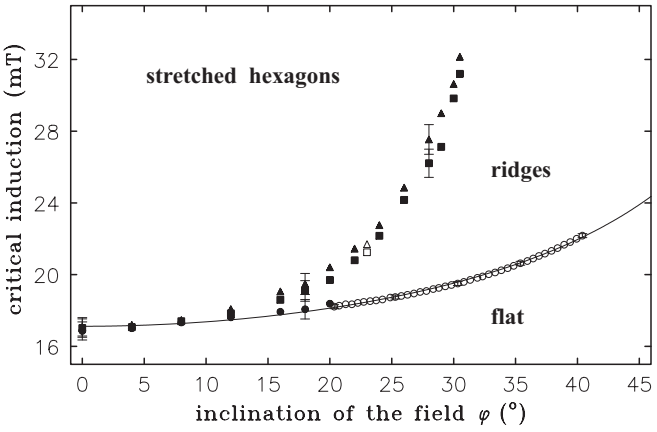

FIG. 7: Critical inductions versus the inclination of the magnetic field. The data marked by open circles have been estimated by fitting the evolution of the ridge amplitude (e.g. Fig. 4) by Eq. (2). The other values, marked by full symbols, have been determined by visual inspection of the liquid layer. The solid line gives the fit obtained via Eq. (10).

Next we investigate the angular dependence of the critical induction for the first and secondary bifurcation. In Fig. 7 the measured data for the transition to ridges are marked by circles, whereas the transition to stretched hexagons is denoted by triangles and the reverse transition to ridges by squares.

The solid line gives B_p calculated for the instability of the flat surface. It follows from the dispersion relation of the surface waves in y-direction with $\omega^2 = 0$ and $k_y = k_c = \sqrt{\rho g/\sigma}$, using the relation between magnetic induction and magnetization,

$$\omega^2(k_x = 0, k_y) = g|k_y| + \frac{\sigma}{\rho}|k_y|^3 - \frac{\mu_0}{\rho}k_y^2 M_Z^2 \times \frac{M^2 - M_Z^2\frac{\bar{\chi}-\chi}{\bar{\chi}+1}}{M^2 - M_Z^2\frac{\bar{\chi}-\chi}{\bar{\chi}+1} + \frac{M}{\bar{\chi}+1}\sqrt{M^2 - M_Z^2\frac{\bar{\chi}-\chi}{\bar{\chi}+1}}}. \quad (10)$$

The dispersion relation Eq.(10) takes into account the nonlinearity of the magnetization curve $M(H)$ of the fluid and can be deduced from Eq.(36) in [11] whereby $\mathbf{M} = M_Z\mathbf{e}_z + M_X\mathbf{e}_x$ denotes the magnetization of the fluid for the undisturbed surface. The susceptibilities $\bar{\chi}(H) = \frac{M(H)}{H}$ and $\chi'(H) = \frac{\partial M(H)}{\partial H}$ were determined from the experimental magnetization curve assuming a logarithmic normal distribution for the size of the magnetic particles in the fluid [12, 13]. In contrast, in Ref. [2] a constant χ has been used, which results in a B_p not depending on φ.

To conclude, for the tilted field instability we have measured the forward bifurcation to liquid ridges. The angular dependence observed in the experiment, is quantitatively described by taking into account the nonlinear magnetization. In addition we measured the backward bifurcation to hexagons, which has been predicted by an energy variational method [2]. A full quantitative agreement with these predictions can not be expected, because the theory is restricted to permeabilities $\mu_r < 1.4$, while we had to use $\mu_r = 2.11$ to avoid huge fields. The essence of the experimental observation, namely a structural change of the primary instability, seems to be well described by this theoretical ansatz: For broken symmetry ridges always precede hexagons. They are increasingly difficult to resolve, however, if the angle of tilt diminishes. A similar scenario can be expected e.g., for non-boussinesq inclined layer convection [14], for magnetohydrodynamic as well as electro-convection in tilted magnetic fields [15], for lucent hexagons under influence of an asymmetric Fourier filter [17], and for Turing patterns [16] in stressed gel.

We thank W.Pesch for fruitful discussions and *Deutsche Forschungsgemeinschaft* for financial support under grant Ri 1054/1-3.

[1] M. C. Cross and P. C. Hohenberg, Rev. Mod. Phys. **65**, 870 (1993).
[2] R. Friedrichs, Phys. Rev. E **66**, 066215 (2002).
[3] R. E. Rosensweig, *Ferrohydrodynamics* (Cambridge University Press, Cambridge, 1985).
[4] M. D. Cowley and R. E. Rosensweig, J. Fluid Mech. **30**, 671 (1967); A. Gailitis, J. Fluid Mech. **82**, 401 (1977).
[5] Y. D. Barkov and V. G. Bashtovoi, Magnetohydrodynamics (N.Y.) **13**, 497 (1977).
[6] B. Reimann, R. Richter, I. Rehberg, and A. Lange, Phys. Rev. E **68**, 036220 (2003).
[7] B. Reimann, *Experimente zur Normal- und Schrägfeldinstabilität magnetischer Flüssigkeiten*, (Shaker Verlag, Aachen, 2003).
[8] R. Friedrichs and A. Engel, Phys. Rev. E **64**, 021406 (2001).
[9] A. Aitta, G. Ahlers, and D. S. Cannel, Phys. Rev. Lett. **54**, 673 (1985).
[10] G. Pfister and I. Rehberg, Physics Letters **83A**, 19 (1981).
[11] R. E. Zelazo and J. R. Melcher, Fluid Mech **39**, 1 (1969).
[12] R. Friedrichs, Ph.D. thesis, Universität Magdeburg, 2003.
[13] J. Embs et al., Magnetohydrodynamics **37**, 222 (2001).
[14] K. E. Daniels, B. B. Plapp, and E. Bodenschatz, Phys. Rev. Lett. **84**, 5320 (2000).
[15] F. H. Busse and R. M. Clever, Eur. J. Mechanics B **9**, 225 (1990). A. Buka, B. Dressel, L. Kramer, and W. Pesch, Phys. Rev. Lett. **93**, 044502 (2004).
[16] Q. Ouyang and H. Swinney, Nature **352**, 610 (1991).
[17] T. Ackemann, B. Giese, B. Schäpers, and W. Lange, J. Opt. B: Quantum Semiclassical Opt. **1**, 70 (1999).